Thermal Properties and Joinability Investigation of BaO–SrO–SiO₂–B₂O₃ Glasses for Oxygen Transport Membrane Application

Xinfang Li,* Sonja M. Groß-Barsnick,* Stefan Baumann, Thomas Koppitz, Wilhelm A. Meulenberg, and Ghaleb Natour

Three new BaO–SrO–SiO₂–B₂O₃ (BS) glasses with different SrO contents (6–25 mol%) are developed for oxygen transport membrane (OTM) joining application. The content of strontium is investigated first in terms of its effect on the glass-forming tendency, thermal expansion coefficient, crystallization, shrinkage behavior, and viscous flow properties. Differential scanning calorimetry (DSC) is carried out. Dilatometric tests are performed to obtain coefficients of thermal expansion (CTEs) of BS glasses. The crystallization behavior of the BS glasses is investigated by X-ray powder diffraction (XRD). Sinking dilatometric measurements simulate the joining procedure and observe the shrinkage behavior of the BS glasses. The viscous flow behavior of the BS glasses is examined via hot stage microscopy. The glass with 15 mol% SrO (BS15) glass shows the best glass-forming tendency, most matching CTE ($11.9 \times 10^{-6}\,K^{-1}$), densest microstructure, highest shrinkage rate (24%), and good viscous behavior at high joining temperatures compared with other BS glasses. BS15 glass is chosen for helium leak test and assembly test joining with Aluchrom and $SrTi_{0.75}Fe_{0.25}O_{3-\delta}$ membrane (STF25). The sandwiched sample with two Aluchrom plates sealed by BS15 glass at 1075 °C for 5 min achieves good gas-tightness with low helium leakage rate $<10^{-9}$ mbar·l·s⁻¹.

1. Introduction

Global warming is mainly caused by carbon dioxide and methane from fossil fuels and industrial processes, which has become the main environmental threat of this century. Oxygen transport membranes (OTMs) are a promising technological choice to relieve the environmental stress from greenhouse gases CO_2 and CH_4.[1] OTMs can be integrated in different membrane reactors,[2] for example, to produce syngas (CO, H_2) from methane[3] or methane/CO_2 mixture[4] and for CO_2 decomposition.[5] At present, $SrTi_{0.75}Fe_{0.25}O_{3-\delta}$ (STF25) is considered to be a promising OTM because of its favorable high chemical stability[6] with suitable flux and excellent mechanical properties.[7–11] In order to apply the OTM to an industrial process, a robust joining technology is needed to assemble membranes and support metals together in a reactor. The sealants should be able to resist long-term operation temperatures higher than 800 °C and also need to meet other requirements, such as matching thermal expansion with the OTM and substrate alloy as well as exhibiting good chemical compatibility, suitable viscous flow properties during joining, suitable rigidity, and appropriate gas tightness.[12]

Glass sealants are excellent candidates for joining materials due to their heat resistance, tunable composition and properties, and good sealing behavior at OTM operation environment (>700 °C).[13] Reis et al.[14] invented the barium–aluminum–silica-based glass sealants which exhibited sufficient coefficient of thermal expansion (CTE) values (11–12.8 ppm °C⁻¹) with oxygen transport membrane. Kiebach et al.[15] reported two types of system

X. Li, S. M. Groß-Barsnick, T. Koppitz, G. Natour
Central Institute of Engineering
Electronics and Analytics – Engineering and Technology (ZEA-1)
Forschungszentrum Jülich GmbH
52428 Jülich, Germany
E-mail: xin.li@fz-juelich.de; s.m.gross@fz-juelich.de

The ORCID identification number(s) for the author(s) of this article can be found under https://doi.org/10.1002/adem.202200660.

X. Li, G. Natour
Faculty of Mechanical Engineering
RWTH Aachen University
52056 Aachen, Germany

S. Baumann, W. A. Meulenberg
Institute of Energy and Climate Research – Materials Synthesis and Processing (IEK-1)
Forschungszentrum Jülich GmbH
52428 Jülich, Germany

W. A. Meulenberg
Faculty of Science and Technology
Inorganic Membranes
University of Twente
7522 Enschede, The Netherlands

**ADVANCED
SCIENCE NEWS**

www.advancedsciencenews.com

**ADVANCED
ENGINEERING
MATERIALS**

www.aem-journal.com

glasses: CaO–ZnO–B_2O_3–SiO_2 glass with CTE $11.2 \times 10^{-6}\,°C^{-1}$ and low Ba containing glass ($\leq 1\%$). Low Ba glass shows a CTE of $6.3 \times 10^{-6}\,°C^{-1}$, being lower than OTM parts. Lamberson et al.[16] investigated four systems of aluminum-containing glass used for alumina membrane. The sealing glasses exhibited CTE values around $10 \times 10^{-6}\,°C^{-1}$. Da Silva et al.[17] investigated BaO–Al_2O_3–SiO_2 glasses modified with B_2O_3 and reported that a $BaAl_2Si_2O_8$ phase was formed after heat treatment at 850 °C. Brendt et al.[18] and Borhan et al.[19] also reported that the same phenomenon was found in barium aluminosilicate system glasses after heat treatment. The addition of Al_2O_3 to glasses causes the formation of undesirable low CTE phase $BaAl_2Si_2O_8$, which would cause a mismatch when joining the glass sealant. Due to this problem, many compositions of glass sealants without Al_2O_3 have been investigated.[20] Rezazadeh et al.[21] fabricated SiO_2–B_2O_3–BaO system glasses with a decent CTE of up to $12.6 \times 10^{-6}\,K^{-1}$, and barium silicate crystalline phases were formed after heat treatment. If a glass sealant includes the same element, Sr, as the STF25 membrane material, it can be expected to reduce diffusion at the interface between the glass sealant and the STF25 membrane through a reduction in the chemical gradient between the components,[22] while their chemical compatibility could be improved. Some strontium silicate phases also have a decent CTE, such as $SrSiO_3$ ($11.4 \times 10^{-6}\,K^{-1}$) and Sr_2SiO_4 ($12.8 \times 10^{-6}\,K^{-1}$).[23] Kim et al.[24] reported SrO–SiO_2–B_2O_3 glass with a CTE of around $9.2 \times 10^{-6}\,K^{-1}$. The literature values of barium silicate phases are reported to have a relatively high CTE, such as $BaSi_2O_5$: $14.1 \times 10^{-6}\,K^{-1}$,[25] $Ba_2Si_3O_8$: $12.6 \times 10^{-6}\,K^{-1}$,[25] and $Ba_5Si_8O_{21}$: $14.5 \times 10^{-6}\,K^{-1}$.[26] Zhang et al.[27] found that the low CTE phase SrB_2O_4 ($8.5 \times 10^{-6}\,K^{-1}$) was formed when borate content is higher than or equal to 30 mol% in on Sr–Ba–borosilicate glasses. The focus of this work is to investigate the effect of SrO on BaO–SrO–SiO_2–B_2O_3 (BS)-based glasses, with the hope of obtaining desirable crystalline phases such as barium silicates, strontium silicates, or Ba–Sr silicate compounds. Moreover, the glass-forming tendency is related to the critical cooling rate and the ability against devitrification. A glass with a higher glass-forming tendency means glass is easily fabricated with a small cooling rate, for example, free cooling in air, and prevents volume crystallization during cooling.[28] Hrubý measured the glass-forming tendency parameter by calculating the relation of the onset crystallization temperature (T_r), the glass transition temperature (T_g), and the onset melting temperature (T_m).[29]

In this work, three BS glasses with different SrO contents were fabricated using the melt-quenching method, and the effect of SrO on the glass-forming tendency, thermal properties, crystallization, and joining behavior was investigated. Differential scanning calorimetry (DSC) measurements were performed to determine the glass formation ability of each BS glass. The thermal expansion coefficients of BS glass were measured to investigate the effect of Sr concentration on the thermal properties of BS glasses. The microstructures of annealed samples were investigated by scanning electron microscopy (SEM) and energy-dispersive X-ray analysis spectroscopy (EDS). In addition, crystalline phases of BS glasses after heat treatment at 850 °C were investigated by X-ray powder diffraction and their influence on the thermal expansion coefficient was discussed. Finally,

the joining ability of BS glasses was assessed by sinking dilatometer, hot stage microscopy (HSM) (TOMMIplus) measurements, helium leak testing, and joining with the STF25 membrane.

2. Experimental Section

The BS glasses with a composition of BaO–SrO–SiO_2–B_2O_3 were prepared using the melt-quenching method and designated as glasses BS6, BS15, and BS25. They were prepared according to the stoichiometric ratio given in **Table 1** by mixing a batch of raw materials ($BaCO_3$, $SrCO_3$, SiO_2, and H_3BO_3) which were purchased from Merck KGaA (Germany) and had a grade of purity higher than 99%. Each batch (100 g) was heated in a platinum crucible at 1500 °C for 3 h with a heating rate of 15 K min^{-1} in an electrically heated chamber furnace (Carbolite 1700, UK) and poured into ice water to form glass. The glass frits were washed in acetone and dried at 60 °C. They were ground in a planetary ball mill to a median particle size of 10–13 μm and tested with a laser particle size analyzer (LA-950). The chemical compositions of the BS glasses were analyzed by inductively coupled plasma optical emission spectroscopy (ICP-OES, ICAP 7600) after alkaline pulping. The results are shown in Table 1. For the amounts of SrO and SiO_2, 2% molar divergence was found in the BS25 glass when comparing the nominal composition with the as-analyzed composition, which may be caused by the preparation process.

DSC measurements were performed to determine the glass formation ability and glass thermal stability of each BS glass. A commercial DSC instrument, Linseis (STA PT 1600), was employed with a heating rate of 15 K min^{-1} up to 1300 °C in an alumina crucible in an air atmosphere. The phase transition temperatures were measured within an accuracy of ± 2 °C.

Dilatometric measurements were performed on BS glasses with a dual rod Linseis L75 dilatometer at a heating rate of 3 K min^{-1}. The dilatometer rods were pressed under a load of 2.5 tons and sintered at 900 °C for 1 h before being cut into 25 mm-long bars. Some of the sintered bars were annealed at 850 °C for 50 h, and then measured with a dilatometer at the same heating rate. Microstructure analyses for the polished cross sections of the annealed dilatometer samples were carried out via SEM (Zeiss Sigma VP) and EDS (X-Max^N, Oxford).

To investigate phase formation at the OTM application temperatures, BS glasses were heated at 850 °C for 50 h on a platinum foil. After being ground in an agate mortar, an X-ray powder diffractometer (XRD, D4 Endeavor, Bruker AXS GmbH) was used to test the powder samples after heat treatment.

Sinking dilatometric measurements were performed in a commercial apparatus Netzsch 402 ES with a specially designed

Table 1. Chemical composition of BS glasses (in mol%).

Composition	Nominal composition [mol%]				As-analyzed composition [mol%]			
	BaO	SrO	SiO_2	B_2O_3	BaO	SrO	SiO_2	B_2O_3
BS6	30	6	54	10	30.1	6.0	53.9	10.0
BS15	30	15	45	10	30.0	14.7	44.9	10.4
BS25	25	25	40	10	24.5	22.8	42.5	10.2
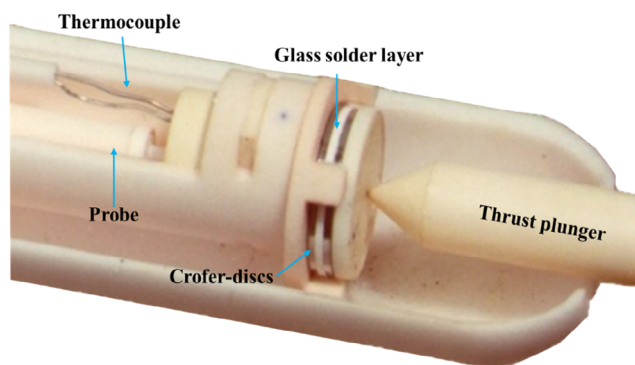
Figure 1. Probe head of the sinking dilatometer.

adapter for applying a load of 261 g at a heating rate of 2 K min^{-1}. The shrinkage behavior of a glass sealant layer is measured by the sensor on the surface of the second steel disk (**Figure 1**) with a resolution of about $\pm 1\,\mu$m.[30] The temperature-, time-, and pressure-dependent glass sealant shrinkage behavior is examined using this measurement and the joining process of an OTM stack is simulated under realistic conditions.[31] To prepare the shrinkage samples, the glass pastes were made by mixing an organic binder solution with glass powders. The pastes were applied on the Crofer22APU wafers (Ø 18, 0.5 mm), and then put into a drying chamber at 60 °C for 3 h. The green layer after drying has a thickness of around 200 μm.

Thermo-optical, HSM (TOMMIplus, Fraunhofer Gesellschaft, Germany) was used in this work to monitor the deformation and melting behavior of candidate glasses BS6, BS15, and BS25 at high temperatures. The pellets (Ø 10 mm) for the TOMMIplus specimens were pressed from BS glass powders with a pellet weight of 1.5 g each. The measurements were conducted at a fast heating rate of 15 K min^{-1} from room temperature to 500 °C and a rate of 5 K min^{-1} to 1100 °C.

For the application of BS glass to a sealing geometry, a paste was prepared by adding BS15 glass powder (82 wt% solid content) to a binder solution consisting of ethyl cellulose and α-terpineol, and blending them thoroughly. The paste was subsequently applied via a syringe-controlled dispenser by Nordson EFD dispensing robots (DR-2503N) on the steel or polyester film surface. The pastes were then dried at 60 °C in a ventilated heating chamber overnight.

In order to investigate the joinability of BS15 glass, a gas-tightness test was performed on the double-layered steel plates and a joining test was carried out on the STF25 membrane and steel plate. VDM Aluchrom Y Hf (1.4767) was chosen as support metal plate with a thickness 1 mm. Here, STF25 wafer was produced by pressing of the calcined STF25 powders and followed by subsequent sintering at 1400 °C for 5 h. The joining process was performed by heating to a temperature of 350 °C at a rate of 2 K min^{-1} and dwelling for 60 min for binder burn-out with a subsequent increase in temperature to 1075 °C for 5 min in air. The gas-tightness test was performed on two steel plates with a size of 48 × 48 mm^2, one of which had a drilled hole with a 10 mm diameter in a sandwiched structure. Using two steel plates joining with glass sealant to evaluate glass sealing behavior, one can avoid the disturbance from other factors, such

as the leakage caused by cracking of STF25 during the heating process, intrinsic permeability as property of STF25 itself, and the interfacial reaction between membrane and glass sealant. The sealant paste was applied in the middle layer of the sandwich. Four small yttria-stabilized ZrO$_2$ (YSZ, KERAFOL—Keramische Folien GmbH) spacers with a thickness of 0.15 μm were placed between the hole of the plate and the sealant foil in order to keep a distance between two plates. The heating process was carried out with a dead load of 800 g on the top steel plate of the sandwiched setup. The gas tightness of the sandwiched samples was evaluated by helium leak testing (UL 200, Inficon). In addition, the sealant foil was placed between the Aluchrom plate and the STF25 membrane wafer (Ø 16 mm). The thickness of the glass sealant foil was around 0.5 mm. The setup was placed into a muffle furnace for the joining process described above and under a dead load of 60 g. The joining performance of the sealants with the STF25 and the steel was evaluated by performing microstructural analysis on the cross sections of the samples with a scanning electron microscope (Zeiss Sigma VP) together with an energy-dispersive X-ray spectrometer (Oxford).

3. Results and Discussion

3.1. Glass-Forming Tendency

Figure 2a–c shows the results of DSC, which was carried out on the quenched glasses BS6, BS15, and BS25 to characterize their thermophysical properties. From the DSC curves, it is possible to determine the characteristic temperatures of BS glasses, such as T_g, T_r, exothermic peak temperature of crystallization (T_p), melting onset temperature (T_m), and endothermic melting peak temperature (T_{mp}), all of which are summarized in **Table 2**. Figure 2d shows the DSC magnification curves of BS glasses between 500 and 800 °C for better visualization of the glass transition temperature (T_g) and crystallization onset temperature (T_r). The T_g values of the BS glasses decrease with increasing strontia content from 637 to 581 °C. Similar findings in the literature on the decline of T_g was explained by the formation of nonbridging oxygens.[32] Moreover, T_r and T_p values decrease with increasing SrO content in BS glasses, which means that BS25 glass has a lower activation energy for crystallization when heating. The BS6 and BS15 glasses have only one distinct exothermal crystallization peak T_p at 778 and 741 °C, respectively. In contrast, the BS25 DSC curve exhibited four crystalline peaks at 717, 755, 904, and 1031 °C, which means that four different crystalline structures would originate before reaching melting temperature. With the measuring temperature rising, BS glasses start to melt. Glass does not have a fixed melting point, but a melting process that continuously absorbs heat. The position of the maximum endothermic peak T_{mp} can be determined. First, the T_{mp} of BS15 is at 1071 °C. Subsequently, the T_{mp} of BS6 is at 1127 °C and BS25 T_{mp} is close to BS6 at around 1133 °C

From the DSC data, the glass-forming tendency and glass thermal stability of each BS glass were evaluated on the basis of the relative onset temperatures of the T_g, T_r, and T_m, which were calculated using the equations proposed by Hrubý (K_{gl}) in 1972.[29]
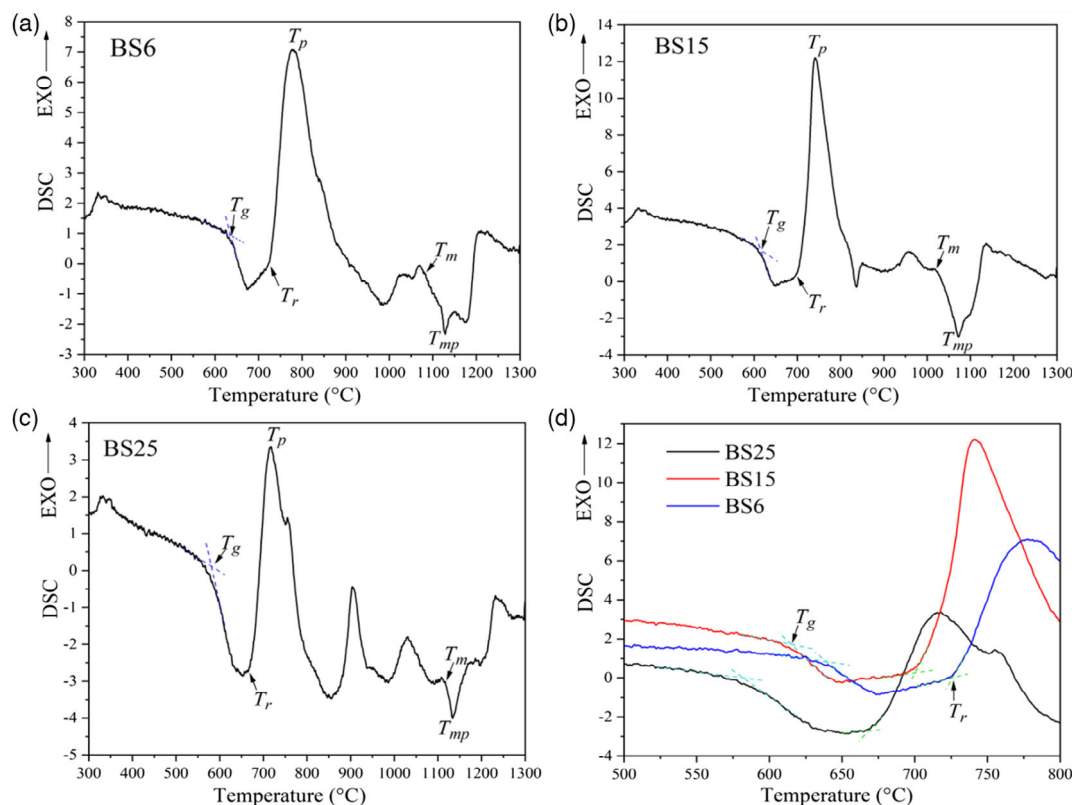
Figure 2. DSC curves of BS glasses at a heating rate of 15 K min^{-1}: a) BS6, b) BS15, c) BS25, and d) magnification of DSC curves between 500 and 800 °C for better visualization of T_g and T_r.

Table 2. DSC data, K_{gl} of BS glasses.

Sample	T_g [°C]	T_r [°C]	T_p [°C]	T_m [°C]	T_{mp} [°C]	K_{gl}
BS6	637	725	778	1083	1127	0.25
BS15	616	700	741	1022	1071	0.26
BS25	581	668	717	1113	1133	0.20

$$K_{gl} = \frac{T_r - T_g}{T_m - T_r} \qquad (1)$$

where $0.1 \leq K_{gl} \leq 1$. If $K_{gl} = 0.1$, the preparation of glass is very difficult and requires additional technical help.[33] For a K_{gl} close to 0.5, glass can be prepared simply by free cooling the melt in air. For $K_{gl} = 1$, glass is a high molecular polymer type.[29]

Table 2 presents the corresponding K_{gl} values of BS glasses. BS15 has the largest K_{gl} value (0.26), which is close to that of BS6 (0.25). $0.20 \leq K_{gl} \leq 0.26$ means that all the BS glasses can be easily prepared under a cooling rate of around 15 °C min^{-1}. BS glasses are still in a glassy state after a DSC measurement cooling procedure of 15 °C min^{-1} (as shown in **Figure 3**), which verifies the above conclusion using the Hrubý Equation (1). Results imply that BS15 has the best glass-forming tendency, resistance against devitrification and thermal stability in three BS glasses.
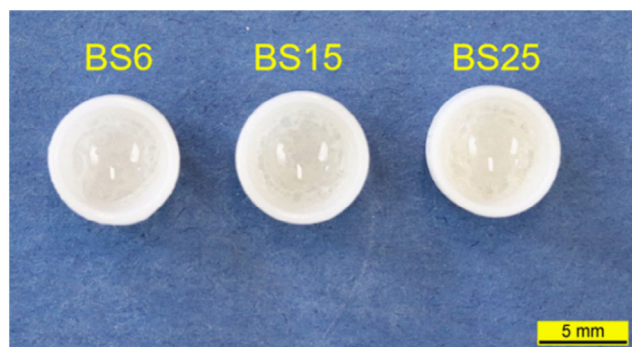
Figure 3. DSC crucibles of BS glasses (cooling rate 15 K min^{-1}).

3.2. Thermal Expansion

The CTEs of BS glasses were measured using a dilatometer with rods sintered at 900 °C for 1 h. The results are presented in **Figure 4** as a) elongation plots, b) calculated CTE values of BS glasses as a function of temperature in comparison with the STF25 membrane and the Aluchrom support metal, and c) the CTE magnification curves of BS15 and BS25. Elongation and CTE curves of BS glasses increased with rising temperature and decreased with an increasing concentration of Sr. In contrast, the dilatometric softening temperature (T_s) of BS glasses rises with increasing Sr concentration—from 835 °C for BS6
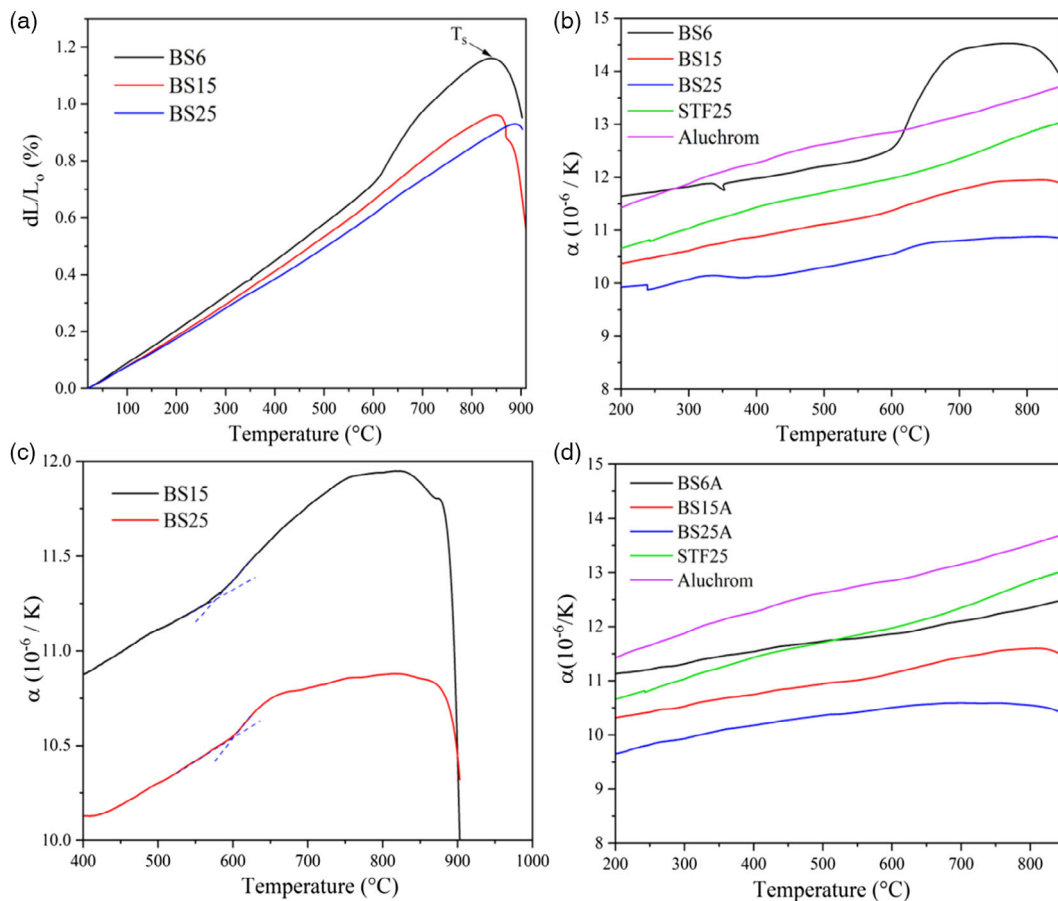
Figure 4. Dilatometer curves of BS glasses: a) elongation plots, dilatometer softening temperature (T_s), b) CTE of BS glasses as a function of temperature compared with STF25 membrane and Aluchrom, c) CTE magnification curves of BS15 and BS25, and d) dilatometer curves of the annealed BS samples after 850 °C for 50 h.

glass to 886 °C for BS25 glass. As the dilatometric softening temperature of all BS glasses is higher than 835 °C, BS glasses should be ideal for use as high-temperature sealants. The respective CTE values in the temperature range from 200 to 850 °C as well as the dilatometric softening temperature T_s and glass transition temperature T_g of the as-sintered BS glasses are summarized in **Table 3**. Dilatometer glass transition temperatures are slightly different from the values measured by DSC, which can be explained by different heating rate of the specific measurement and partial crystallization of the dilatometer rods of as after sintering of pressed BS glass powders. BS6 resulted in the highest CTE value (up to 14.5×10^{-6} K^{-1}) compared with BS15 and BS25, even higher than the CTE of the STF25 membrane

Table 3. Thermal properties of as sintered BS glasses measured by dilatometer.

Sample	T_g [°C]	T_s [°C]	CTE [10^{-6} K^{-1}] (200–850 °C) sintered	CTE [10^{-6} K^{-1}] (200–850 °C) annealed
BS6	601	835	11.6–14.5	11.1–12.5
BS15	582	846	10.4–11.9	10.3–11.6
BS25	599	886	9.9–10.9	9.7–10.6

($10.7–13.1 \times 10^{-6}$ K^{-1}). The CTE plot of Aluchrom intersects with the BS6 curve at 617 °C, and the CTE value of BS6 is higher than Aluchrom in the range of 617–855 °C. The step increase of the CTE of BS6 at 600 °C is due to the typical change of property at the glass transition zone. The steep decrease in the CTE of BS6 after 810 °C can be attributed to the initial softening of the dilatometric glass rod. A similar phenomenon was also observed for BS15 and BS25. The CTEs of the BS15 ($10.4–11.9 \times 10^{-6}$ K^{-1}) and BS25 ($9.9–10.9 \times 10^{-6}$ K^{-1}) glasses were slightly lower than Aluchrom ($11.4–13.8 \times 10^{-6}$ K^{-1}) and STF25. The coefficient of thermal expansion decreases with the increasing SrO content of the BS glasses. This finding was expected because the substitution of the network modifier BaO as the bigger cation with SrO as the smaller cation in a composition produces a smaller CTE in silicate glasses.[20]

Figure 4d presents the dilatometer curves of the annealed BS glass samples after thermal treatment at 850 °C for 50 h. The annealed samples exhibited highly ceramic behavior of the material, as no glass transition point T_g is visible. Moreover, the CTE of the annealed samples decreases with increasing strontium, which is in accordance with the regularity of measurement of short-term sintered BS glasses. The CTE values of the annealed samples decreased slightly when compared to the BS glasses

**ADVANCED
SCIENCE NEWS**

www.advancedsciencenews.com

**ADVANCED
ENGINEERING
MATERIALS**

www.aem-journal.com

sintered at 900 °C for 1 h. A comparison of expansion values is given in Table 3. The decrease of CTE is likely a result of the formation of low CTE phases, which is why a detailed investigation of the crystallization behavior was carried out by following SEM and XRD analyses. The cross sections of the annealed BS dilatometric specimens are depicted in **Figure 5**. The annealed BS15 specimen shows the highest compaction with a dense microstructure and minimal porosity compared to BS6 and BS25. When comparing the differences, there are some crystalline phases precipitated from BS glasses after annealing. An EDS elemental mapping of BS6 is presented in **Figure 6**. It is hard to distinguish between the phases in the EDS mapping. The crystallization behavior of the annealed samples at 850 °C for 50 h is analyzed by XRD in Section 3.3.

3.3. Crystallization

All three BS glasses were heated at 850 °C for 50 h, and XRD analysis was carried out in order to investigate phase formation and to analyze their possible influence on the thermal expansion coefficient. The XRD patterns of the BS glasses are shown in **Figure 7**. The main crystalline phases precipitated in the heated

BS6 glass (Figure 7a) were two binary barium silicates ($BaSi_2O_5$ and $Ba_5Si_8O_{21}$) and a ternary barium strontium silicate ($BaSrSi_3O_8$), while tiny amounts of low quartz (α-SiO_2) were also present after heat treatment at 850 °C. Similar crystalline behavior was observed for the BS15 glass in Figure 7b. The phases present after heat treatment of the BS15 sample were $Ba_5SrSi_{10}O_{26}$, $Ba_2Si_3O_8$ $Ba_2SrB_6O_{12}$, and tridymite. Barium strontium boride ($Ba_{1.84}Sr_{1.16}$) (B_3O_6)$_2$, SrO, and α-SiO_2 precipitated in BS25 glass (Figure 7c).

We listed crystallographic information of polymorphism SiO_2 phases formed in BS glasses in **Table 4**. BS6 and BS25 glasses formed same low quartz phase in principle, even though they have different PDF cards. Low quartz (α-SiO_2) and syn low quartz have the same crystal structure, space group, and space group number. Hexagonal tridymite was identified in the annealed BS15, which is a high-temperature phase comparing with low quartz. From the literature, pure tridymite is formed and stable at high temperatures between 867 and 1470 °C.[34] In complex system such as glass-ceramic[35] and kaolin,[36] tridymite formation was observed beginning at 600 °C.

Binary Ba/Si phases have relatively high thermal expansion coefficients, which are reported to be $BaSi_2O_5$: 14.1×10^{-6} K^{-1},[25]
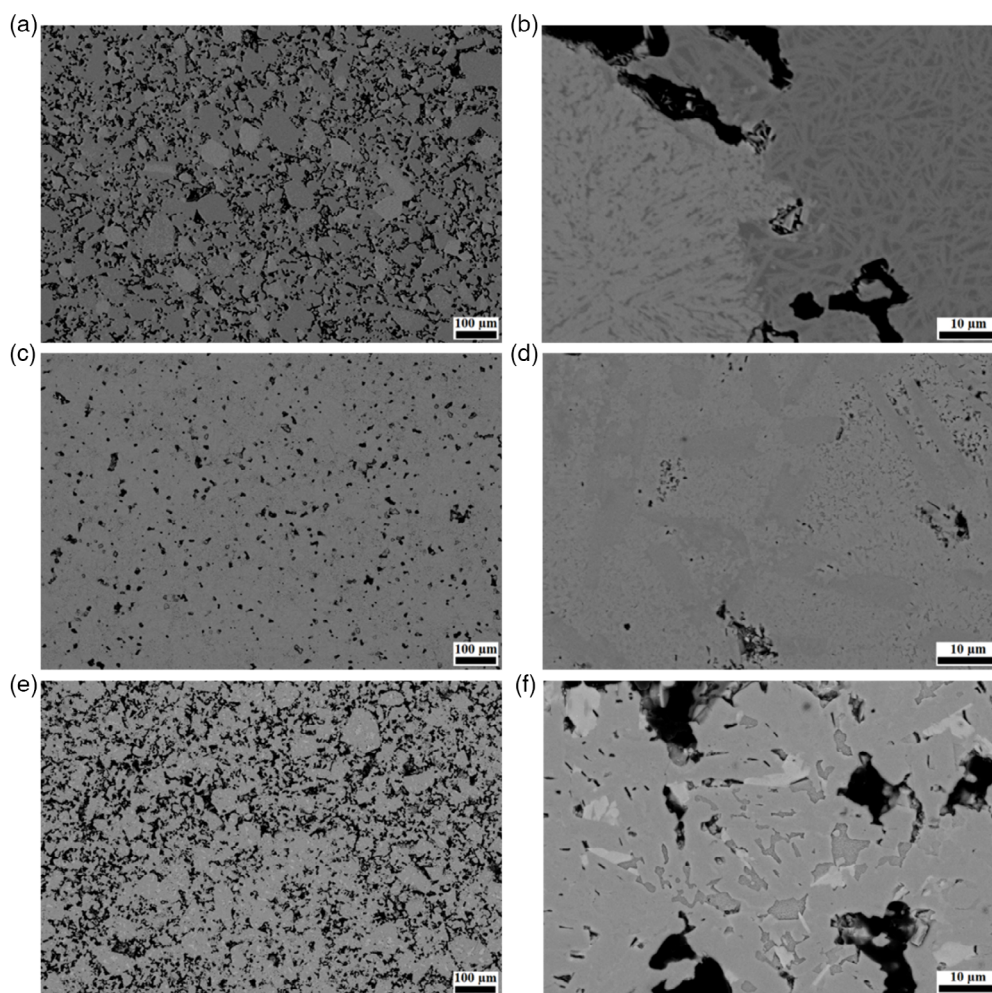
Figure 5. SEM images of the annealed dilatometer samples: a,b) BS6A, c,d) BS15A, and e,f) BS25A; overview on the left and magnification on the right.
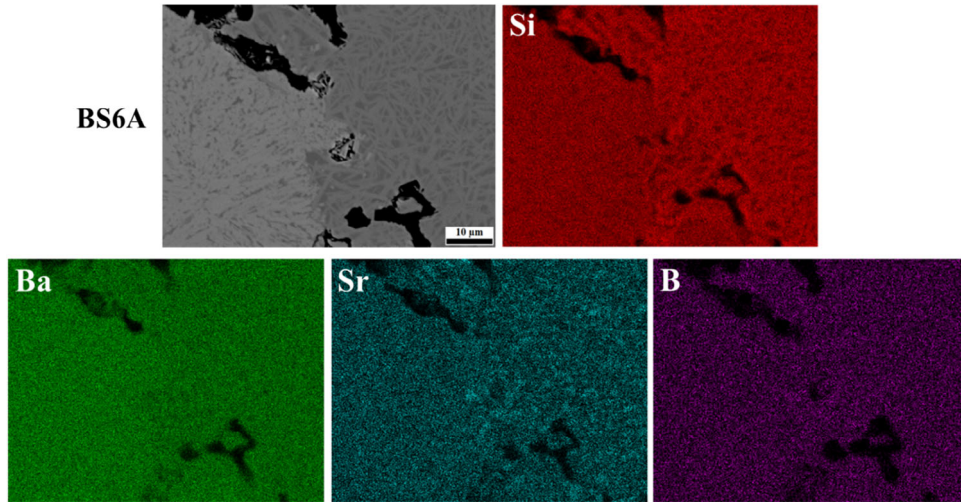
Figure 6. EDS maps of the annealed sample BS6A after sintering at 900 °C for 1 h and thermal treatment at 850 °C for 50 h.
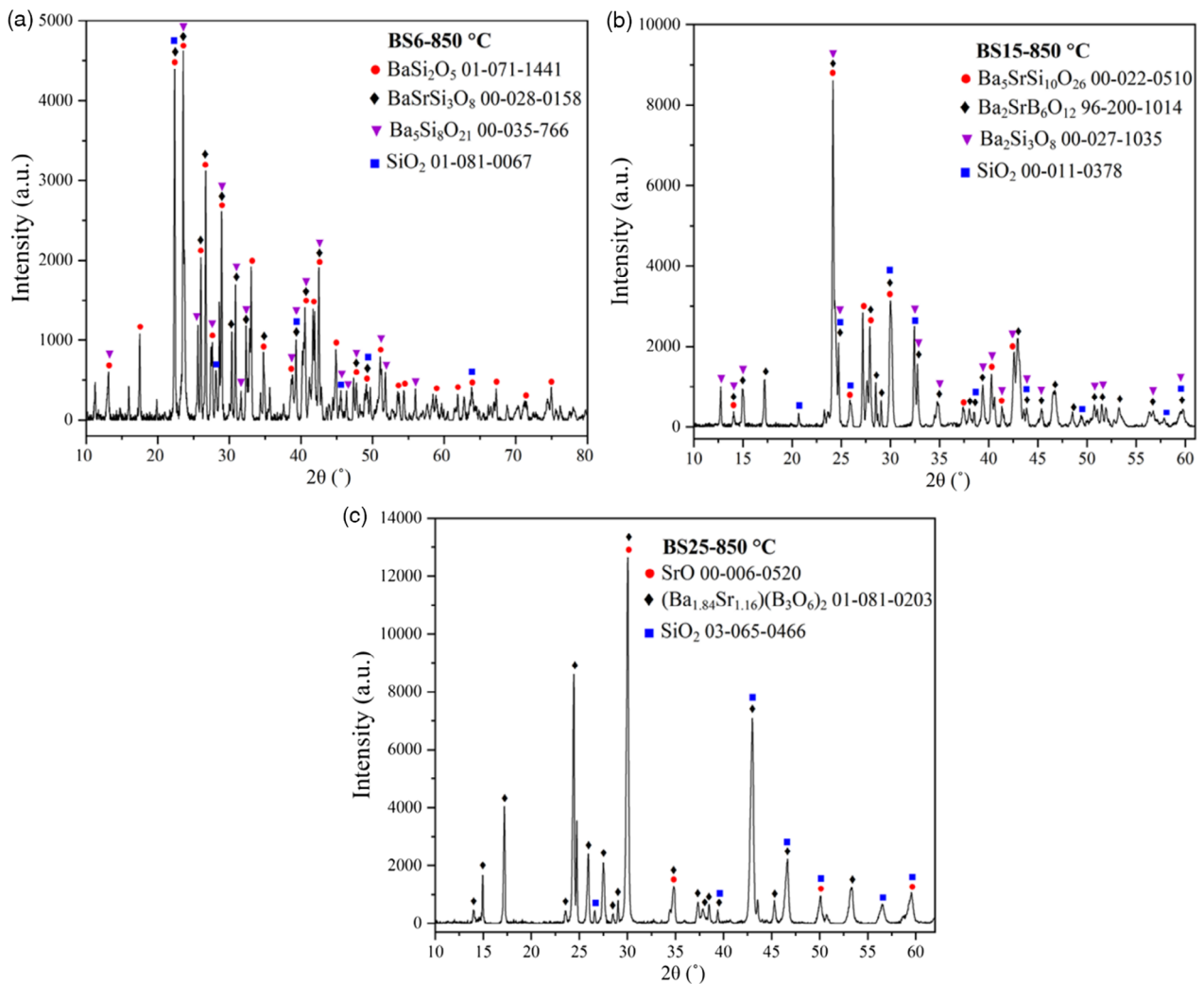
Figure 7. XRD patterns of BS glasses heated at 850 °C for 50 h: a) BS6, b) BS15, and c) BS25.

Table 4. The crystallographic information of polymorphism SiO_2 phases formed in BS glasses.

Sample	PDF card	Mineral name	Crystal structure	Space group	Space group number
BS6	01-081-0067	Quartz low (α-SiO_2)	Hexagonal	P3221	154
BS15	00-011-0378	Tridymite	Hexagonal	P63/mmc E	194
BS25	03-068-0466	Quartz low, syn	Hexagonal	P3221	154

$Ba_2Si_3O_8$: 12.6×10^{-6} K^{-1},[25] and $Ba_5Si_8O_{21}$: 14.5×10^{-6} K^{-1}.[26] In contrast, the binary Sr/Si phases have a comparably lower CTE than the Ba/Si compounds, such as $SrSiO_3$: 11.2×10^{-6} K^{-1}.[23] Ternary Ba/Sr silicates were also formed. A small amount of SiO_2 (α-SiO_2: 10.5×10^{-6} K^{-1},[37] tridymite: 10–4×10^{-6} K^{-1}[38]) with lower CTE values was found for all of the BS glasses after heat treatment at 850 °C, which would decrease thermal expansion property of the sealants.

These findings could explain the slight decrease of the CTE values of BS glasses after annealing at 850 °C, as shown in the dilatometer curves of Figure 4c. Barium silicate phases, barium–strontium silicate phases, and strontium silicate phases are desirable phases in crystallized BS-based glass due to their relatively high CTE values, which might enable the sealing of OTM components such as Aluchrom and STF25. With the increase in SrO content in BS glasses, Sr^{2+} replaces Ba^{2+} in some cases, which is why some Ba/Sr compounds were formed in three BS glasses after heat treatment at 850 °C, such as barium strontium silicates and barium strontium borides. It is worth noting that the formation of borate-containing crystalline phases, for example, $Ba_2SrB_3O_{12}$ and $(Ba_{1.84}Sr_{1.16})(B_3O_6)_2$, reduces the vitreous B_2O_3 content in the glass matrix. The capture of B_2O_3 in a crystalline phase is expected to lead to good stability against volatilization and thus an improvement in the thermal stability of the resulting glass ceramic is also expected.[27] Furthermore, alkaline-earth boride phases have a possible self-healing behavior in glass sealants.[39]

3.4. Joinability

3.4.1. Sinking Dilatometer

Sinking dilatometric measurements were able to simulate the stack joining conditions and the shrinkage behavior of BS glasses was observed in between two steel plates under a constant pressure of 10 KPa. **Figure 8** shows the shrinkage behavior for three different BS glass solders. Onset shrinking temperature (T_a), end shrinking temperature (T_b), and the maximum shrinkage rate of BS glasses are listed in **Table 5**. BS6 glass underwent a sharp shrinkage process from T_a 717 °C to T_b 786 °C. Below 717 °C, BS6 only showed slight shrinkage of less than 3%. The shrinkage curve of BS6 then remained steady after T_b until the end of the measurement. BS15 glass has a similar shrinking process to BS6 and showed the highest shrinkage rate (about 24% at 850 °C) compared with the other BS glasses. BS25 exhibited the lowest shrinkage rate (around 15%). The shrinkage rates of BS glasses are lower than that of glass H, with 39% reported in previous investigations.[40] The shrinkage is due to sintering densification and compaction of the powder as well as the viscous behavior of the glass at high temperatures.
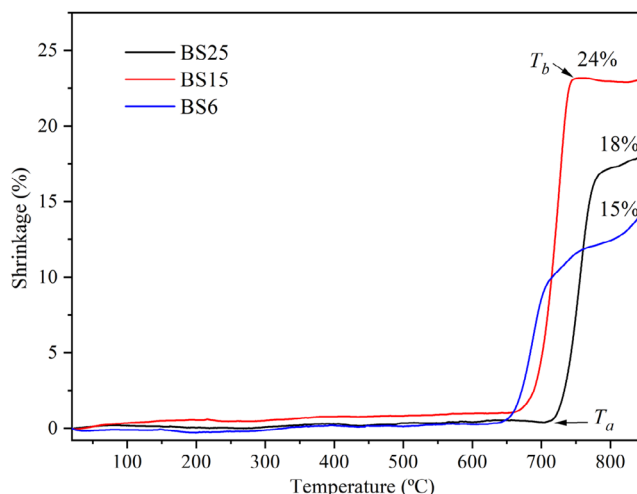
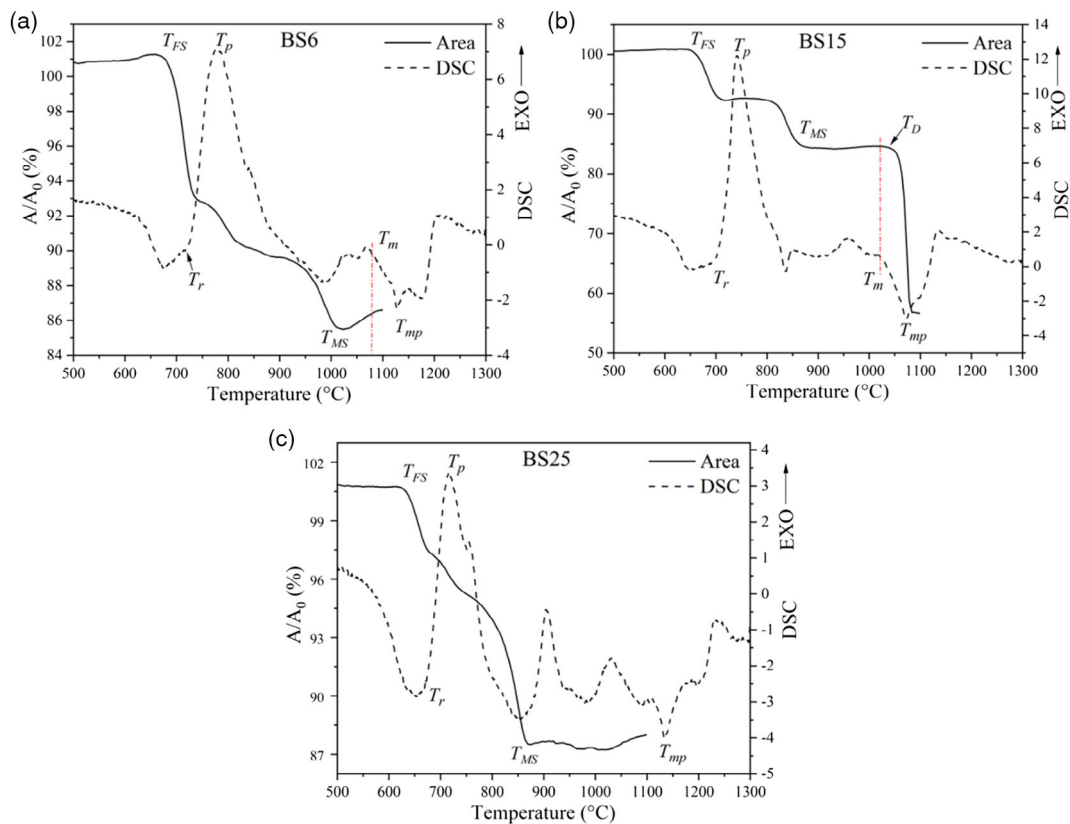**Figure 8.** Sinking dilatometry plots of BS glasses.

Table 5. Onset shrinking temperature T_a, shrinking end temperature T_b, and shrinkage rate at 850 °C.

Sample	T_a [°C]	T_b [°C]	Shrinkage 850 °C
BS6	717	786	18%
BS15	665	748	24%
BS25	654	753	15%

3.4.2. HSM

Figure 9 shows HSM and DSC curves of the powdered BS glasses: a) BS6, b) BS15, and c) BS25. The fixed viscosity temperatures[41] can be obtained from the HSM results, such as first shrinkage temperature (T_{FS}), maximum shrinkage temperature (T_{MS}), deformation temperature (T_D), half ball temperature (T_{HB}), and flow temperature (T_F). **Table 6** summarizes the temperature values (T_{FS}, T_{MS}, T_D, T_{HB}) and the area shrinkage rates at T_{MS} for the different BS glasses obtained by TOMMIplus measurements.

Comparing HSM and DSC results in the same temperature range shows how the composition affects sintering, devitrification phenomena, and the melting behavior of glasses, and enables the suitable joining temperature for OTM application to be determined. BS glasses exhibited a similar trend with this procedure, i.e., crystallization points T_r and T_p occur between the onset shrinkage stage T_{FS} and the final sintering stage T_{MS}. In **Figure 10**, it can be seen that where the crystallization appears, the area shrinkage rates of the curves slow down, or there is even a plateau stage. The crystallization phenomena appear before complete shrinkage/densification is obtained, which means it could prevent further sintering. With the SrO composition increasing, the T_{FS} and T_{MS} of the BS glasses decline, respectively. The maximum shrinkage temperature of the BS6 glass is up to 1018 °C. BS15 and BS25 have similar T_{MS} values (878, 868 °C). BS15 glass shows the highest area shrinkage rate at the maximum shrinkage point (A_{MS}/A_0), which is around 84.4%.

ADVANCED
SCIENCE NEWS
www.advancedsciencenews.com

ADVANCED
ENGINEERING
MATERIALS
www.aem-journal.com

Figure 9. HSM and DSC curves obtained from the powdered BS glasses: a) BS6, b) BS15, and c) BS25.

Table 6. HSM data of BS glasses.

Sample	T_{FS} [°C]	T_{MS} [°C]	T_D [°C]	T_{HB} [°C]	A_{MS}/A_0
BS6	675	1018	–	–	85.5%
BS15	650	878	1033	1075	84.4%
BS25	633	868	–	–	87.5%

In contrast, no deformation or flow point of the BS6 and BS25 glasses takes place under 1100 °C. According to their DSC plots, BS6 and BS25 could melt around 1130 °C. Figure 10 shows the shadow images of BS15 glass on the Crofer22APU substrate from HSM. The deformation temperature (T_D) of BS15 occurs after the melting onset temperature (T_m), and the half ball point (T_{HB}) is at 1075 °C. From Figure 10, it can be seen that the optimal joining temperature of BS15 glass should be around the maximum melting peak temperature (T_{mp}), 1071 °C, between T_D and T_{HB}. The half ball temperature of the BS glass is higher than 1000 °C, which is advantageous for high-temperature (HT) joining applications.

3.4.3. Helium Leak Testing for the Joint

In accordance with the previous investigation, BS15 glass was chosen for helium leak testing and assembly test joining with

Aluchrom and STF25 due to their relatively high CTEs (11.9×10^{-6} K^{-1}), dense microstructure, highest shrinkage rate (24%), and good viscous behavior at high temperatures compared with other BS glasses.

As a next step, a gas leakage experiment was first performed to verify the joinability of the BS15 sealant with the Aluchrom substrate. In accordance with HSM analyses for BS15 glass, the joining process was chosen at 1075 °C for 5 min. The sample sealed by glass sealant BS15 showed very good gas-tightness with a helium leakage rate lower than the detection limit of 10^{-9} mbar·l s^{-1}. According to the indications of Mahapatra et al., the sealant with a gas leakage rate of lower than 10^{-7} mbar·l s^{-1} would fulfill the requirements for the high-temperature operation of the OTM module.[42] In order to check inner joining structure, the gas-tight joint Aluchrom/BS15/Aluchrom was cut open. The macroscopic and magnified images of the joint are presented in **Figure 11**. The joint exhibits a very dense joining structure (Figure 11b), and no crack or defect could be found. This joint setup was separated with difficulty, and the mechanical force that was applied significantly exceeded the strength of YSZ, meaning that the YSZ spacers were torn, as shown in Figure 11c. In contrast, the BS15 glass sealant achieved good wettability and excellent adherence to Aluchrom. BS15 should have good mechanical properties. The specific mechanical test will be carried out in future.

SEM images of the cross sections of the gas-tight Alchrom/BS15/Aluchrom joint are shown in **Figure 12**. No large pores
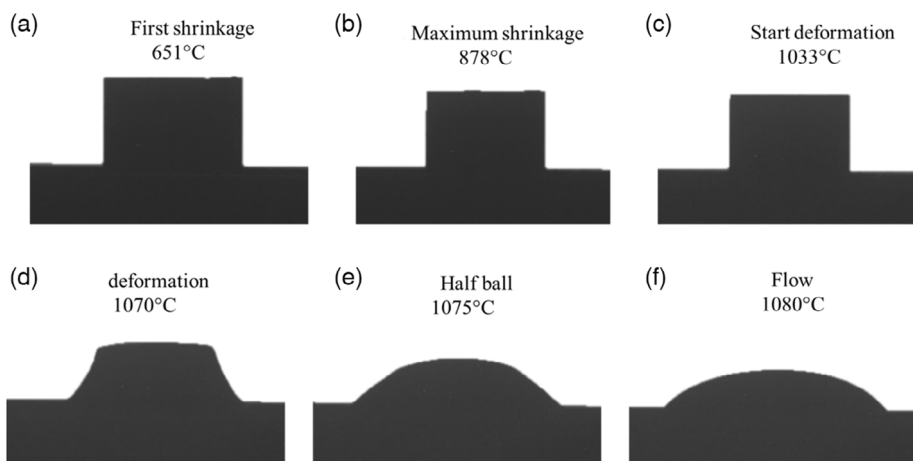
**ADVANCED
SCIENCE NEWS**

www.advancedsciencenews.com

**ADVANCED
ENGINEERING
MATERIALS**

www.aem-journal.com

Figure 10. Shadow images of BS15 glass pellet on Crofer22APU substrate from HSM.
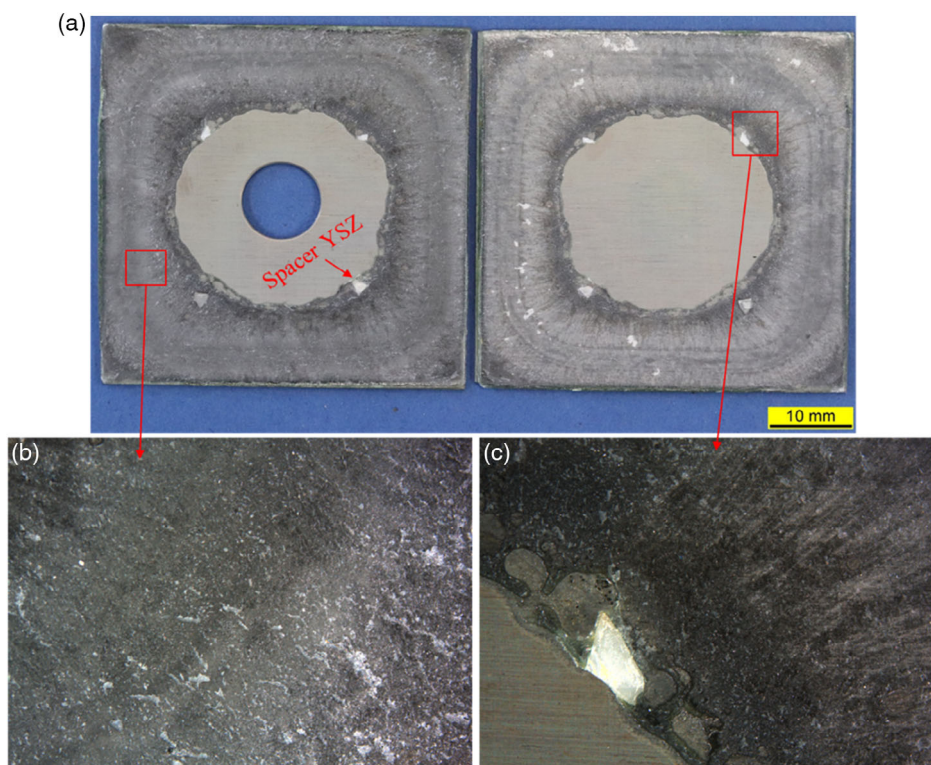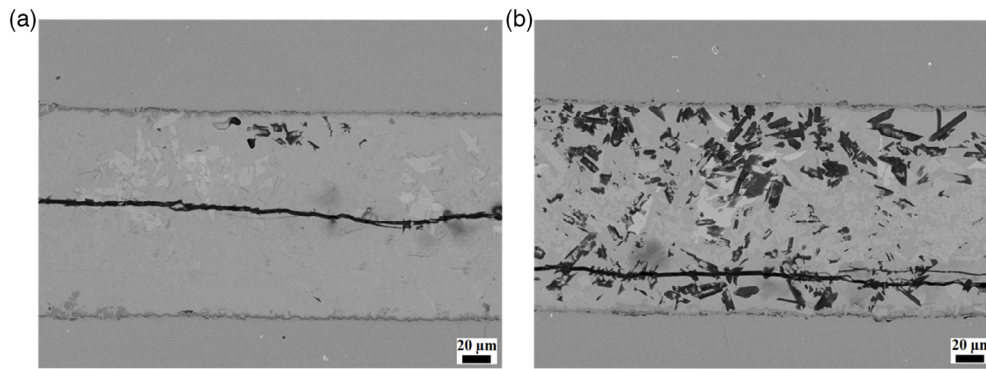

Figure 11. The cut-open images of the gas-tight joint Alchrom/BS15/Aluchrom sealing at 1075 °C for 5 min: a) overview; b,c) magnification.

were detected from the SEM analysis. However, obvious cracks were found in the sealant. As no cracks were found in Figure 11 and the joint showed excellent gas tightness, it is concluded that the cracks were formed during metallographic processing, such as cutting and grinding. Moreover, Figure 12a,b shows two different areas of the same joint. Inhomogeneous structures were observed for the two different parts of BS15, which could be explained by the phase segregation in the pure glass sealant. For the interfaces of the BS15 glass sealant and Aluchrom,

BS15 glass achieved excellent adherence to Aluchrom, and there was no crack, or formation of pores found at the two interfaces. **Figure 13** shows SEM-EDS maps of the gas-tight Aluchrom/BS15/Aluchrom joint after joining at 1075 °C for 5 min to analyze crystalline phases from the BS15 sealant and the interdiffusion layer of BS15 and Aluchrom. Aluchrom formed a thin scale layer, which is assumed to be Cr/Al oxide scale from the mapping images. The black columnar pointed phase is assumed to be quartz with a small amount of Sr diffusion inside. Some crystal

**ADVANCED
SCIENCE NEWS**

www.advancedsciencenews.com

**ADVANCED
ENGINEERING
MATERIALS**

www.aem-journal.com

Figure 12. SEM images of the gas-tight joint Aluchrom/BS15/Aluchrom sealing at 1075 °C for 5 min: a,b) show inhomogeneous structures.
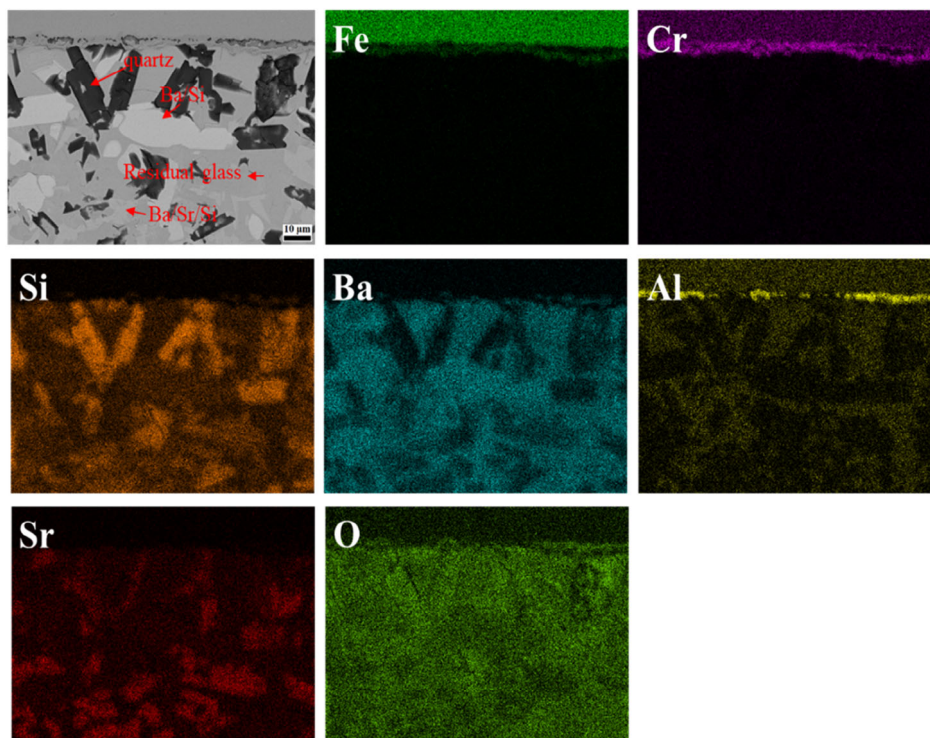
Figure 13. SEM-EDS maps of the gas-tight joint Alchrom/BS15/Aluchrom joined at 1075 °C for 5 min to analyze the crystalline phases from the BS15 sealant and the interaction layer of BS15 and Aluchrom.

phases also formed from the BS15 glass, such as the Ba silicate phase and the Ba–Sr silicate phase. The SEM-EDS mapping results are in good agreement with the XRD result of BS 15 (Figure 7c).

Figure 14 shows interfacial microstructure and EDS mapping of Aluchrom and glass sealant BS15. One can see the formation of a Al$_2$O$_3$ scale followed by a chromia sublayer which is in a good agreement with literature.[43] A schematic diagram of the interface reaction between BS15 glass sealant and Aluchrom joined at 1075 °C for 5 min was shown in **Figure 15**. Besides, the scale oxidized at interface of Aluchrom has been partially dissolved by BS15 glass during high-temperature joining process. Internal corrosion of the steel leads to Fe/Cr nodules precipitation and

the interface is composed of the two zones of island-like steel residues with Alumina-enriched glass-ceramic adjacent to the Aluchrom.

3.4.4. Assembly Test with STF25 Membrane

The assembly of the experiment with OTM and Aluchrom was also investigated to verify the joinability of the BS15 for further applications. **Figure 16**a shows the assembly before joining. The glass sealant green foil stamped to a suitable size was placed in the middle of the Aluchrom and the STF25. In contrast, there is a severe reaction and spallation between the BS15 glass and the STF25 membrane and Aluchrom after joining for 5 min at
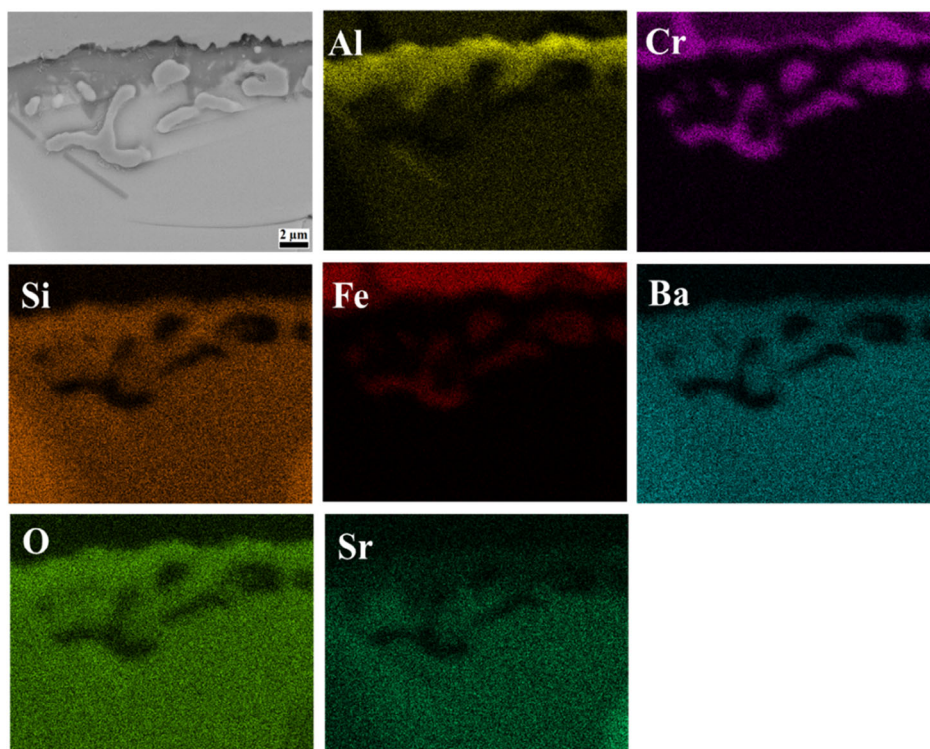
Figure 14. SEM-EDS maps of the gas-tight joint Alchrom/BS15/Aluchrom joined at 1075 °C for 5 min to analyze interaction between BS15 glass and Aluchrom.
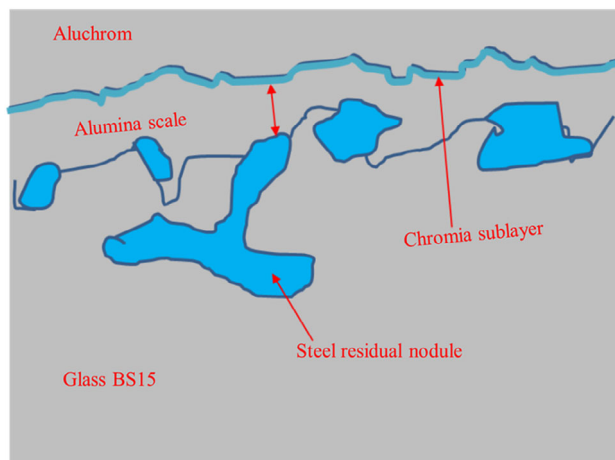
Figure 15. Schematic diagram of the interface reaction between BS15 glass sealant and Aluchrom joined at 1075 °C for 5 min.

1075 °C, as shown in Figure 16b–d. The dark green part visible in Figure 16c can be assumed to be BS15 glass, as shown in SEM image of **Figure 17**a of glass sealant layer. From the literature, observation of a color change (to green) is associated with the formation of a chromia sublayer under the alumina scale,[43] which coincides with Aluchrom/BS15 interfacial analysis (Figure 14). There is a hypothesis that chromium ions diffuse into glass sealant layer at high temperature, so that the color

of glass BS15 changes to green. From Figure 17b the side view of the broken BS15/STF25 part, BS15 displayed good adherence with STF25 at interface. However, the surface of BS15/STF25 shows a red–yellow reaction product which has a coloring similar to rusty. In the STF25 ($SrTi_{0.75}Fe_{0.25}O_{3-\delta}$) membranes, Fe^{3+} and essentially smaller amounts of Fe^{4+} predominantly exist.[44] The Fe–O band of high valences Fe^{4+} shows metallic behavior.[45] Moreover, according to investigations by Silva et al.,[7] a hexagonal (Sr, Fe)-rich secondary phase $SrFe_{12}O_{19}$ was identified in STF25, with the exception of the cubic perovskite phase, which may cause the inhomogeneous phase distribution, rust color, and severe reaction with the BS15 glass at a high temperature over 1000 °C.

There are two possible ways to solve the reaction problem between BS15 and STF25. First, the joining temperature could be reduced to around 900 °C. Another possible strategy is to use the coated membrane SF25, such as yttria-stabilized zirconia (YSZ) coating. Some literatures have studied oxygen transport membrane of YSZ showed high chemical, mechanical stabilities[46–48] and good compatibility with other membranes such as $LaCrO_3$[46] and $SrCo_{0.4}Fe_{0.6}O_{3-\delta}$.[49] Future studies are necessary to investigate the possibility of these two strategies and their interfacial reaction behavior.
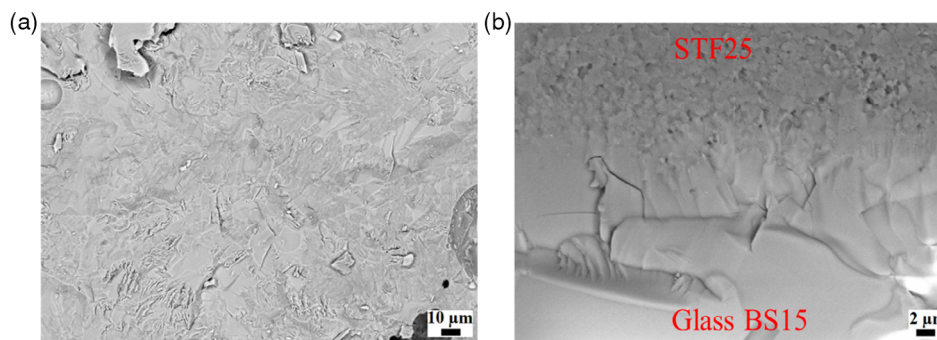
4. Conclusions

Three new BS glasses (BS6, BS15, and BS25) with different SrO contents were fabricated using the melting quenching method.
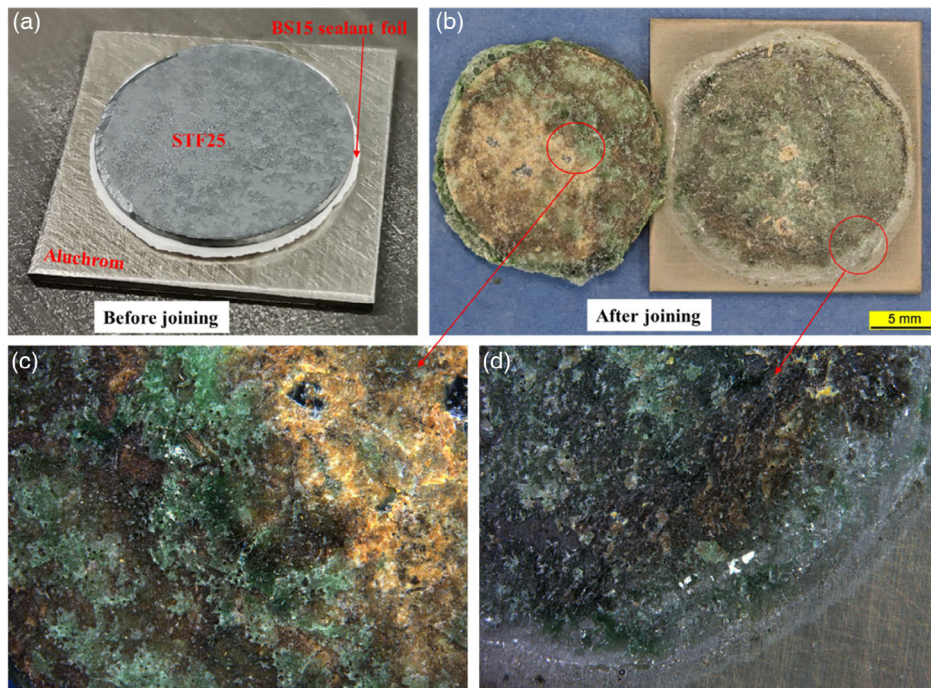
Figure 16. BS15 sealant joining with Aluchrom and STF25 membrane (1075 °C, 5 min): a) before joining, b) after joining, c) zoomed-in picture of the membrane side, and d) zoomed-in picture of the Aluchrom side.

Figure 17. SEM images of BS15/STF25 part from the assembled joint shown in Figure 16c, a) top view on glass sealant layer; b) side view after breaking of the BS15/STF25 piece.

The content of strontium was investigated first in terms of its effect on the glass-forming tendency, thermal expansion coefficient (CTE), crystallization, shrinkage behavior, and viscous flow properties. T_g, T_r, and T_p values of BS glasses decrease with increasing strontia content. BS15 glasses have the best glass-forming tendencies and thermal stability in three BS glasses. The CTE value decreases with the increasing SrO content of the BS glasses. BS6 reached the highest CTE values of up to $14.5 \times 10^{-6} \, K^{-1}$. The glass with 15 mol% SrO (BS15) achieved the most matching CTE of $11.9 \times 10^{-6} \, K^{-1}$ with STF25 and Aluchrom. Ba/Sr compounds were formed in three BS glasses after heat treatment at 850 °C. Besides, BS15 glass shows the densest microstructure, highest shrinkage rate (24%), and good viscous behavior at high joining temperatures compared with other BS glasses. Thus, BS15 glass was chosen for helium leak test and assembly test joining with Aluchrom and STF25. The

optimal joining temperature of the BS15 glass was chosen at close to half-ball temperature. The sandwiched sample sealed by BS15 glass at 1075 °C for 5 min achieved excellent gas-tightness with low helium leakage rate $<10^{-9} \, mbar \cdot l \, s^{-1}$ and dense microstructure when joining with Aluchrom. Unfavorable strong interaction and spallation was observed in the assembly test joining of BS15 glass with STF25. Lowering the joining temperature and trying to coat oxygen transport membrane will be investigated in the future to solve this problem.

Acknowledgements

Conflict of Interest

The authors declare no conflict of interest.

Data Availability Statement

The data that support the findings of this study are available on request from the corresponding author. The data are not publicly available due to privacy or ethical restrictions.

Keywords

glass sealant, joinability, oxygen transport membrane, thermal properties

[1] K. Zhang, J. Sunarso, Z. P. Shao, W. Zhou, C. H. Sun, S. B. Wang, S. M. Liu, *RSC Adv.* **2011**, *1*, 1661.

[2] W. Deibert, M. E. Ivanova, S. Baumann, O. Guillon, W. A. Meulenberg, *J. Membr. Sci.* **2017**, *543*, 79.

[3] W. A. Meulenberg, F. Schulze-Kuppers, W. Deibert, T. Van Gestel, S. Baumann, *Chem. Ing. Tech.* **2019**, *91*, 1091.

[4] K. Zhang, G. R. Zhang, Z. K. Liu, J. W. Zhu, N. Zhu, W. Q. Jin, *J. Membr. Sci.* **2014**, *471*, 9.

[5] Y. L. Luo, T. Liu, J. F. Gao, C. S. Chen, *Mater. Lett.* **2012**, *86*, 5.

[6] Y. Liu, V. Motalov, S. Baumann, D. Sergeev, M. Müller, Y. J. Sohn, O. Guillon, *J. Eur. Ceram. Soc.* **2019**, *39*, 4874.

[7] R. O. Silva, J. Malzbender, F. Schulze-Kuppers, S. Baumann, O. Guillon, *J. Eur. Ceram. Soc.* **2017**, *37*, 2629.

[8] R. O. Silva, J. Malzbender, F. Schulze-Kuppers, S. Baumann, M. Kruger, O. Guillon, *J. Eur. Ceram. Soc.* **2018**, *38*, 5067.

[9] R. O. Silva, J. Malzbender, F. Schulze-Kuppers, S. Baumann, M. Kruger, O. Guillon, *J. Eur. Ceram. Soc.* **2018**, *38*, 2774.

[10] V. V. Kharton, A. V. Kovalevsky, E. V. Tsipis, A. P. Viskup, E. N. Naumovich, J. R. Jurado, J. R. Frade, *J. Solid State Electrochem.* **2002**, *7*, 30.

[11] A. Murashkina, V. Maragou, D. Medvedev, V. Sergeeva, A. K. Demin, P. Tsiakaras, *Energy* **2012**, *37*, 14569.

[12] X. Li, S. M. Groß-Barsnick, T. Koppitz, S. Baumann, W. A. Meulenberg, G. Natour, *J. Eur. Ceram. Soc.* **2022**, *42*, 2879.

[13] M. Kerstan, C. Thieme, A. Kobeisy, C. Russel, *J. Mater. Sci.* **2017**, *52*, 1789.

[14] S. T. Reis, M. J. Schwartz, M. Zandi, Y. Narendar, US10658684B2 **2020**.

[15] W.-R. Kiebach, P. V. Hendriksen, WO2014049119A1 **2014**.

[16] L. A. Lamberson, R. M. Morena, US20110268976A1 **2011**.

[17] M. J. Da Silva, J. F. Bartolome, A. H. De Aza, S. Mello-Castanho, *J. Eur. Ceram. Soc.* **2016**, *36*, 631.

[18] J. Brendt, S. M. Gross-Barsnick, C. Babelot, G. Natour, *J. Non-Cryst. Solids* **2018**, *501*, 78.

[19] A. I. Borhan, M. Gromada, G. G. Nedelcu, L. Leontie, *Ceram. Int.* **2016**, *42*, 10459.

[20] C. Lara, M. J. Pascual, A. Durán, *J. Non-Cryst. Solids* **2004**, *348*, 149.

[21] L. Rezazadeh, S. Baghshahi, A. N. Golikand, Z. Hamnabard, *Ionics* **2014**, *20*, 55.

[22] K. Singh, T. Walia, *Energy Res.* **2021**, *1*, 20559.

[23] C. Thieme, C. Russel, *J. Mater. Sci.* **2015**, *50*, 5533.

[24] E. A. Kim, H. W. Choi, Y. S. Yang, *Ceram. Int.* **2015**, *41*, 14621.

[25] K. S. Weil, J. E. Deibler, J. S. Hardy, D. S. Kim, G. G. Xia, L. A. Chick, C. A. Coyle, *J. Mater. Eng. Perform.* **2004**, *13*, 316.

[26] M. Kerstan, C. Russel, *J. Power Sources* **2011**, *196*, 7578.

[27] T. Zhang, Q. Zou, *J. Eur. Ceram. Soc.* **2012**, *32*, 4009.

[28] A. A. Cabral, C. Fredericci, E. D. Zanotto, *J. Non-Cryst. Solids* **1997**, *219*, 182.

[29] A. Hruby, *Czech. J. Phys.* **1972**, *22*, 1187.

[30] D. G. Frank Caspar, T. Koppitz, *Verfahren und Vorrichtung zur Messung der eindimensionalen Wärmeausdehnung bzw.-schrumpfung einer Probe unter Druckbelastung*, Deutschland **2001**.

[31] U. D. P. Batfalsky, T. Koppitz, in *High Temperature Brazing and Diffusion Welding the 5th Inter. Conf.*, DVS, Aachen, Germany **1998**, pp. 97–99.

[32] S. Y. Kim, J. Park, S. H. Kim, L. Kadathala, J. H. Baek, J. H. Kim, J. H. Choi, *Appl. Sci.* **2020**, *10*, 353.

[33] A. Hrubý, L. Štourač, *Mater. Res. Bull.* **1971**, *6*, 465.

[34] T. J. Rockett, W. R. Foster, *Am. Mineral.* **1967**, *52*, 1233.

[35] X. Y. Liu, Y. P. Pu, P. K. Wang, Z. J. Dong, Z. X. Sun, Y. Hu, *Mater. Lett.* **2014**, *128*, 263.

[36] M. Sellami, M. Barre, M. Toumi, *Appl. Clay Sci.* **2019**, *180*, 105192.

[37] J. A. Kosinski, J. G. Gualtieri, A. Ballato, in *Thermal-Expansion Of Alpha-Quartz, 45th Annual Symp on Frequency Control*, IEEE, Los Angeles, CA **1991**, pp. 22–28.

[38] J. B. Austin, *J. Am. Chem. Soc.* **1954**, *76*, 6019.

[39] T. Zhang, D. A. Tang, H. W. Yang, *J. Power Sources* **2011**, *196*, 1321.

[40] T. K. Sonja, M. Gross, J. Remmel, J.-B. Bouche, U. Reisgen, *Fuel Cells Bull.* **2006**, *2006*, 12.

[41] M. J. Pascual, L. Pascual, A. Duran, *Phys. Chem. Glasses* **2001**, *42*, 61.

[42] K. Eichler, G. Solow, P. Otschik, W. Schaffrath, *J. Eur. Ceram. Soc.* **1999**, *19*, 1101.

[43] M. J. Bennett, R. Newton, J. R. Nicholls, H. Al-Badairy, G. J. Tatlock, *High Temperature Corrosion and Protection of Materials 6, Prt 1 and 2, Proceedings* (Eds: P. Steinmetz, I.G. Wright, G. Meier, A. Galerie, B. Pieraggi, R. Podor) **2004**, pp. 463–472.

[44] E. O. Filatova, Y. V. Egorova, K. A. Galdina, T. Scherb, G. Schumacher, H. J. M. Bouwmeester, S. Baumann, *Solid State Ion.* **2017**, *308*, 27.

[45] G. Demazeau, B. Buffat, M. Pouchard, P. Hagenmuller, *Z. Anorg. Allg. Chem.* **1982**, *491*, 60.

[46] J. M. Lee, G. M. Choi, *J. Eur. Ceram. Soc.* **2007**, *27*, 4219.

[47] K. L. Scholl, E. A. Fletcher, *Energy* **1993**, *18*, 69.

[48] A. Q. Pham, T. H. Lee, R. S. Glass, in *Solid-State Ionic Devices Symp. 195th Electrochemical-Society Meeting*, Seattle, WA **1999**, pp. 172–180.

[49] S. G. Lia, W. Q. Jin, N. P. Xu, J. Shi, *J. Membr. Sci.* **2001**, *186*, 195.